Cycle Adaptive Feedforward Approach Controllers for an Electromagnetic Valve Actuator

Jimmy Tsai, *Student Member, IEEE*, Charles Robert Koch, *Member, IEEE*, and Mehrdad Saif, *Senior Member, IEEE*

***Abstract*—An electromagnetic valvetrain for an internal combustion engine can improve the engine thermal efficiency but requires soft landing control to avoid excessive wear and acoustic noise. To simplify the soft landing problem, the valve control algorithm is partitioned into approach and landing controllers. The landing control is responsible for the last part of the 8 mm valve travel while the approach control is responsible for the rest. This paper focuses on the approach control. The goal of the approach control is to achieve an end state that sets constant initial conditions for the landing control. In addition to an identified system model, information based on previous valve events is utilized to take advantage of the repetitive nature of the valve opening/closing. Nonlinear iterative learning, terminal iterative learning, and Nelder Mead direct search algorithms are three cyclic adaptive feedforward approach controllers that are tested in simulation for automotive electromagnetic valves. These results are compared but the emphasis of this paper is on the Nelder Mead approach which works well both in simulation and experiment for disturbances that are slow compared to the valve travel time.**

***Index Terms*—Internal combustion engine, iterative methods, nonlinear programming, nonlinear systems, solenoids, tracking.**

I. Introduction

THE decoupling between crankshaft and engine valve operation presents an area of potential improvement for the internal combustion engine. If this coupling is removed, the engine valve timing can be optimized at different operating conditions using variable valve timing (VVT) [1], [2]. While many VVT systems are available, there is a strong motivation to develop camless valvetrains [3] which promise improved engine performance, emissions, and fuel efficiency. Various actuators that are consideredfor camshaft replacement include: hydraulic [4], rotary motor [5], piezoelectric type [6], electro-pneumatic [7], and electromagnetic solenoid [8].

This work is based on an electromagnetic valve actuator (EMV) because of its advantages in cost, efficiency, and ruggedness [9]. The advantages of the EMV actuator come from its structural simplicity and the use of springs to recover kinetic energy. The EMV actuator used in this study consists of two evenly-tensioned springs, two solenoids, and one shaft that connects a metal armature to the valve (see Fig. 1). Solenoids are used for holding the armature at either end of the actuator to keep the valve open or closed. To transition between open and closed, current is cut off from the holding solenoid and the armature accelerates and decelerates due to the spring force. The other solenoid (catching solenoid) is then activated to land and hold the armature. Much of the energy needed for travel is stored in the springs and is recovered with the electromagnetic force being used to overcome friction.

The main disadvantage of the EMV actuator is the difficulty to control valve lift. The control problem arises from both the steep decline of magnetic force with respect to distance and the rise of back-EMF related inductance as the armature swings toward the catching coil [11]. Moreover, the limited input voltage (in this case we use 42 V) constrains the magnitude and bandwidth of the magnetic force since the rate of current change is limited. As a result, EMV actuators can suffer from excessive valve landing speed which gives rise to unacceptable wear and acoustic noise [12].

To meet these challenges, the controller objectives should be very different depending on the air gap (distance between the armature and the catching solenoid, denoted as $\mathbf{h}$. At a small air gap where significant magnetic force can be generated, the armature should be controlled to follow a smooth landing trajectory. At a large air gap, the electromagnetic force is small so the controller has little immediate influence over armature position; however, the cumulative effect over time of this force can compensate armature energy shortfall and provide a feasible starting condition for the landing control.

Thus, it is expedient to break the control problem into two parts based on the air gap. When the armature is close to the catching coil, smooth landing is obtained by having the landing controller track a desired trajectory. Over the remaining trajectory, the approach controller operates to provide constant initial conditions needed for the subsequent landing control.

A velocity position phase diagram is shown in Fig. 2 where the solid line is an ideal trajectory and the dashed-dot line is a disturbed trajectory. The important location in Fig. 2 is at 1.45 mm air gap, where the approach control ends and the landing control starts

$$\mathbf{h}^{i}_{\text{land}} = \mathbf{h}^{f}_{\text{appr}} = 1.45 \text{ mm}.$$

The superscripts and subscripts i, f, $land$, and $appr$ stand for "initial", "final", "landing control", and "approach control", respectively. The dashed line connecting the disturbed to the ideal valve lift in Fig. 2 represents the approach controller trajectory

Manuscript received April 17, 2010; revised September 11, 2010; accepted January 15, 2011. This work was supported by Daimler AG and Auto21 Networks of Centres of Excellence of Canada.

J. Tsai was with the School of Engineering Science, Simon Fraser University, Vancouver, BC V5A 1S6, Canada. He is now with the Department of Electrical and Computer Engineering, University of Toronto, Toronto, ON M5S 3G4, Canada (e-mail: jimmy.tsai@utoronto.ca).

C. R. Koch is with the Department of Mechanical Engineering, University of Alberta, Edmonton, AB T6G 2G8, Canada (e-mail: bob.koch@ualberta.ca).

M. Saif is with the School of Engineering Science, Simon Fraser University, Vancouver, BC V5A 1S6, Canada (e-mail: saif@ensc.sfu.ca).

Color versions of one or more of the figures in this paper are available online at http://ieeexplore.ieee.org.

Digital Object Identifier 10.1109/TCST.2011.2126575

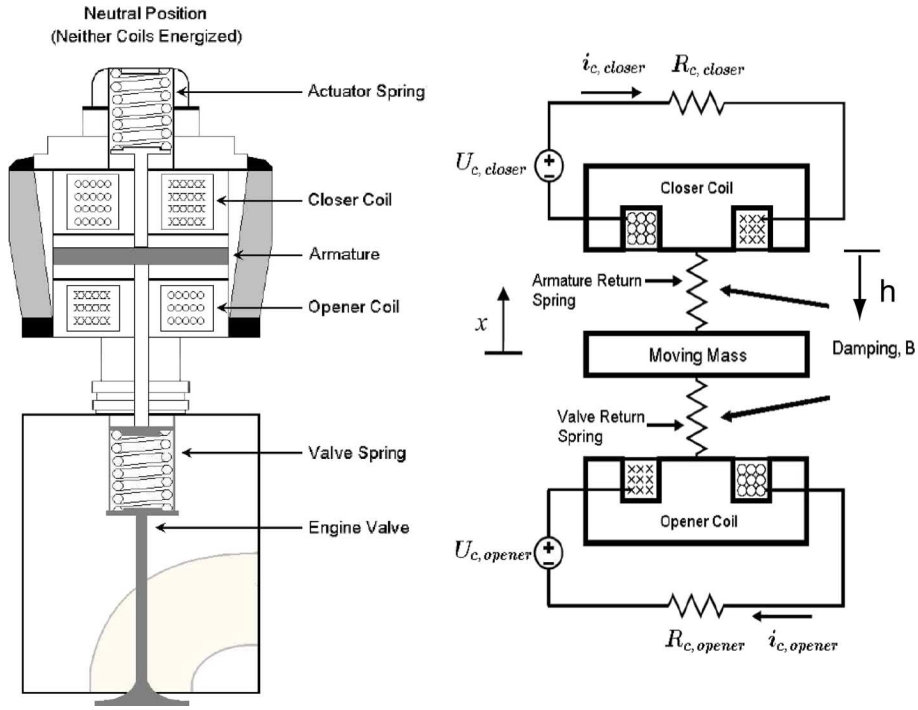

Fig. 1. EMV actuator: (left) section and (right) schematic [10].

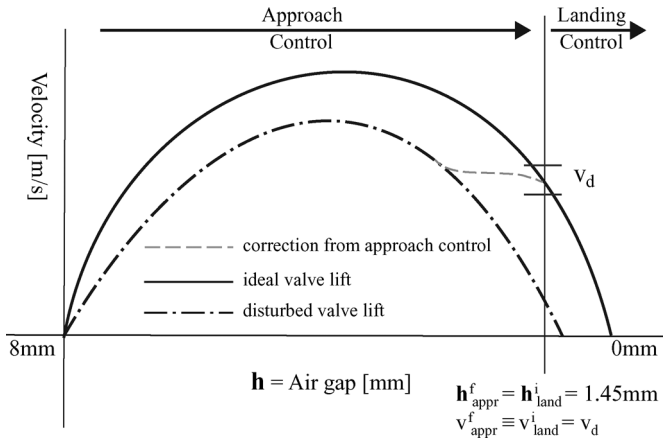

Fig. 2. Control regions for approach and landing control: setting consistent initial conditions for the EMV landing control.

so that disturbances are rejected and at $\mathbf{h}^f_{\rm appr}$ the velocity v and current i are regulated around desired values

$$v^f_{\rm appr} \equiv v^i_{\rm land} = v_d, \quad i^f_{\rm appr} \equiv i^i_{\rm land} = i_d.$$

The value of 1.45 mm air gap and the other states are heuristically chosen based on the mechanical and electromagnetic properties of this valve and being able to generate a feasible trajectory for the landing control—as detailed in [8].

Two types of feedforward control can be employed to achieve this goal: disturbance-estimator based and cycle adaptive. When large cycle to cycle force variations are present, due for example to a single misfire causing a large in-cylinder pressure drop, a disturbance estimation-based controller has been shown to achieve desirable results [13]. When the disturbance dynamic is much slower ($>100\times$) than the valve travel time, cyclical adaptation can take advantage of the information from previous control iterations (valve opening/closing cycle). Examples of this kind of variation are temperature and valve wear. In this paper, cycle adaptive control is developed to reject these slow disturbances.

EMV actuator control has been extensively investigated. To facilitate "sensorless control", a simplified relationship between current measurement and the ratio of armature velocity over position, which require no position or velocity measurements, is presented in [14]. A linear quadratic optimal controller based on a linearized system model is used in [15]. Performance of [14] is improved by adding in takeoff and approach control [16]. Another way to achieve "sensorless control" is through flux-based position reconstruction [17]. Sliding mode control of the EMV actuator is presented in [18] and [19]. While all the above controllers achieve certain performance goals, they can be further optimized by incorporating cycle-adaptation such as repetitive learning control [15], iterative learning control [20], and extremum seeking control [11], [21].

With the goal of improving the cycle-adaptive control, two iterative learning controllers (ILCs), both nonlinear and terminal, as well as a direct search controller are investigated in this paper. Unlike the ILC valve controllers reported in [15] and [20] that rely on linearized models for trajectory tracking, nonlinear ILC aims to achieve tracking convergence without the linearization while terminal ILC utilizes feedback linearization-based integration to regulate $v^f_{\rm appr}$ and $i^f_{\rm appr}$ without trajectory tracking. Nelder Mead achieves the same result as terminal ILC but avoids input saturation by using direct search optimization instead of integration. Compared to [11], nonlinear ILC, terminal ILC, and Nelder Mead allow tuning of multiple coefficients for greater optimization. Last, our system operates under the constraints

TABLE I
EMV ACTUATOR MODEL VARIABLE AND PARAMETER

symbol	name	symbol	name
U_c	voltage	x	armature position
i_c	coil current	i_e	eddy current
R_c	coil resistance	R_e	eddy current resistance
v	velocity	K_s	spring constant
m	mass	$f(x)$	$2\xi_1/(\xi_2 - x) + \xi_3$
B	damping constant	L_e	eddy current inductance
λ_s	saturation flux	ξ_1, ξ_2, ξ_3	curve-fit constants
λ	magnetic flux	$\mathbf{h}$	air gap

of ±42 V supply voltage, and springs with 150 Hz natural frequency. The voltage limit lowers the system bandwidth and increases the risk of input saturation. To obtain valve travel time needed for engine speeds of 5000–6000 rpm, stiff springs are needed which increase the control bandwidth.

II. MODEL FOR THE EMV ACTUATOR

The lumped-parameter model of the valve [8] comes from parameterizing the finite-element model in [22]. The model describes only the catching solenoid and assumes that the release solenoid exerts no force (only one coil is on at a time)

$$\frac{dx}{dt} = v \tag{1}$$

$$\frac{dv}{dt} = \frac{1}{m}\left[\frac{\lambda_s f'(x)}{f^2(x)}\left[1 - [1 + i_c f(x)]\, e^{-i_c f(x)}\right]\right] - K_s x/m - Bv/m \tag{2}$$

$$\frac{di_c}{dt} = \frac{e^{i_c f(x)}}{\lambda_s f(x)}\left[U_c - R_c[i_c + i_e]\right] - \frac{f'(x)}{f(x)} i_c v \tag{3}$$

$$\frac{di_e}{dt} = \frac{1}{L_e(x, i_c)}\left[U_c - R_c(i_c + i_e) - R_e(x, i_c) i_e\right] \tag{4}$$

$$\lambda(x, i_c) = \lambda_s\left(1 - e^{-i_c f(x)}\right) \tag{5}$$

$$F_{\text{mag}} = \frac{\delta}{\delta x}\int_0^{i_c} \lambda(x, \eta)\delta\eta. \tag{6}$$

The model variables and parameters are listed in Table I. During valve opening and closing, the armature position x is at the rest position at an air gap of 4 mm from each side and is related to $\mathbf{h}$ and total valve travel κ (8 mm) as

$$\mathbf{h} = \kappa/2 + x \ \text{(opening)}, \quad \mathbf{h} = \kappa/2 - x \ \text{(closing)}. \tag{7}$$

Equation (5) defines how the magnetic flux $\lambda(x, i_c)$ is related to the saturation flux through the curve fitting function $f(x)$. Magnetic force can then be derived from $\lambda(x, i_c)$ in (6). For greater accuracy, this model accounts for flux saturation and eddy current dynamics. Due to the difficulty in determining R_e, the eddy current dynamics in (4) is considered as a disturbance and is neglected in the model-based design procedure.

A. Initial Conditions of the Approach Control

The desired conditions at the end of the approach control in this paper are defined as the desired initial condition from the flatness-based EMV landing controller in [8] and [10]. Calculated from (1)–(3), position-magnetic force curves for the EMV actuator at different current levels are shown in Fig. 3. At the end of the approach control, $\mathbf{h}^f_{\text{appr}} = 1.45$ mm, the magnetic force starts to increase significantly so that an effective trajectory tracking based landing control for this system can be implemented.

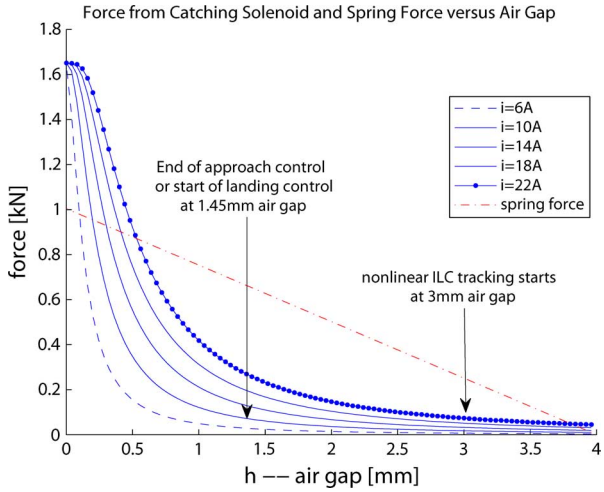

Fig. 3. Magnetic and spring force with respect to the distance between armature and catching solenoid.

TABLE II
FLATNESS LANDING CONTROLLER SIMULATION UNDER VARYING INITIAL CONDITIONS FROM [10]

case	$\mathbf{h}^i_{land}$	v^i_{land}	result
reference	1.45mm	2.59m/s	impact < 0.1m/s
landing control starts early	1.47mm	2.58m/s	impact=0.097m/s
landing control starts early	1.49mm	2.59m/s	impact=0.17m/s
landing control starts late	1.44mm	2.57m/s	failed to land

An error in initial condition of the landing control, translates into an error in landing velocity for the flatness-based controller [10]. An indication of the sensitivity of the landing control to initial conditions can be seen in Table II, where variations in initial conditions cause an increase in impact velocity and even failure for the armature to land. This is why the approach controller is implemented—to provide consistent starting conditions for the landing controller. (Note in Table II, $\mathbf{h}^i_{\text{land}}$ is not fixed. If it was fixed, the tolerance for the velocity at end of approach control will be approximately ±0.1 m/s).

III. ITERATIVE LEARNING CONTROLLERS (ILC)

To provide context for this work and to compare the results to the literature, two iterative learning controllers are briefly detailed for this EMV system. These two methods perform poorly in simulation, and so, they are not implemented in hardware, but a short summary of the possible reasons is given.

A. Nonlinear ILC

The ILC work proposed in [20] is first investigated for approach control. For increased robustness in comparison to the operating point based linearization [20], the convergence result

of the nonlinear ILC from [23] is used. This assumes a system with continuous dynamics and discrete observation

$$\dot{z}(t) = F\left(z(t), u(t)\right), \quad y(j\triangle) = G\left(z(j\triangle)\right). \tag{8}$$

The function $F(z(t), u(t))$ defines how state vector $z(t)$ changes from input $u(t)$, while $G(z(j\triangle))$ relates the output from the state vector at sample interval $\triangle$ and index j. The controller described in [23] is of an error integrator form for kth iteration

$$u_{k+1}(j\triangle) = \Phi_k(j\triangle)\left[e_k((j+1)\triangle) - \sum_{i=0}^{\mu-1} \frac{\triangle^i}{i!} e_k^{(i)}(j\triangle)\right] + u_k(j\triangle) \tag{9}$$

where u is the control input, $e^{(i)}$ is the ith derivative of the tracking error, Φ is the learning gain, and μ is the relative degree of the system. For the EMV system, the input is the solenoid command voltage, and the tracking error comes from the position sensor.

It is shown in [23] that for the tracking error to converge, the learning gain $\Phi_k(j\triangle)$ must be selected such that

$$1 > \left|1 - \frac{\triangle^\mu}{\mu!}\Phi_k(j\triangle) d_k(j\triangle)\right| \tag{10}$$

$$d_k(j\triangle) = \sup\left[\frac{d}{du} L_f^{\mu-1} G\left(z_k(j\triangle), u(k)\right)\right] \tag{11}$$

where $z_k(j\triangle)$ is the EMV state vector comprising position, velocity, and solenoid current. The variable d_k represents the maximum bound for how input affects output derivative, and is computed by taking Lie derivative of the function $G(z_k(j\triangle), u(k))$ to one less the system relative degree μ. Due to the low magnetic force beyond 3 mm air gap, see Fig. 3, the nonlinear ILC applied to the EMV actuator only tracks a trajectory between the 3 to 1.45 mm air gap ($\mathbf{h}^f_{\text{appr}}$).

B. Terminal ILC

The Terminal ILC method used here follows ILC development in semi-conductor wafer processing [24], and wheeled robot trajectory planning [25]. Unlike the nonlinear ILC which tracks the entire trajectory, the terminal ILC considers only the two end states: current i^f_{appr} and velocity v^f_{appr} at the end of approach control. If the magnetic force F_{mag} can be directly influenced, then the EMV system becomes a linear mass-spring damper system. To linearize the system, the relation between magnetic force and current (6), is inverted so that the input current is a function of the desired magnetic force as

$$i_{\text{des}} = \frac{1}{f(x)}\left[W_{-1}\left(\frac{F_{\text{mag}} f^2(x)}{\lambda_s f'(x) - 1}\right) + 1\right] \tag{12}$$

where the function W_{-1} is the Lambert W function [26]. The desired current profile is approximated through an on-off voltage controller (to emulate the H-bridge hardware). Further, the magnetic force profile during one valve event is parameterized through a third order B-spline interpolation, which reduces the dimensions of input vector C to eight coefficients. Most importantly, these two techniques enable the prediction of the valve states at the end of approach control

$$X(T) = V_n(T)X(0) + W_n(T)C \tag{13}$$

where $X(T)$ is the predicted linearized states at time T, and $V_n(T), W_n(T)$ are matrices that depend only on time. A more detailed analysis of the predictor from (13) is given in [27]. The Terminal ILC updates the control coefficient C through the following update law:

$$C_{k+1} = C_k + L\epsilon_k \tag{14}$$

where L is the learning gain, and $\epsilon_k = X_d - X_k$ denotes the terminal error at iteration k. The convergence of the algorithm is based on the evolution of the error. The error of the next iteration, ϵ_{k+1}, is described in terms of the current error, ϵ_k, by combining the predictor (13) and the update law (14) to derive the following:

$$\epsilon_{k+1} = \left(I - W_n(T)L\right)\epsilon_k. \tag{15}$$

The above error equation shows that under ideal conditions the terminal errors will reduce monotonically provided that the learning gain is selected such that each eigenvalue of matrix $(I - W_n(T)L)$ is less than unity. Thus the learning matrix, L, is chosen to be the pseudo-inverse of $W_n(T)$.

C. Discussion for Both ILCs

Both iterative learning controllers show convergence in simulation provided that the input voltage constraint of 42 V is removed. With this input constraint imposed, neither controller performs satisfactorily [27]. A systematic way to determine trajectories despite input saturation is needed in order for nonlinear ILC to be useful. For terminal ILC to be successful, a procedure to steer the linearized coefficients to evolve away from the constraints is needed. Thus methods to select $G(z_k(jh), u(k))$ and $W_n(T)$ subject to the constraints could be topics of future work.

IV. Nelder Mead Simplex Algorithm

One way to take advantage of the repetitive nature of the EMV actuator is to optimize the quadratic cost function of errors at the end of approach control using the outcomes of previous valve cycles as functional evaluations

$$F(c) = \left(\alpha\left(v^f_{\text{appr}}(c) - v_d\right)^2 + \beta\left(i^f_{\text{appr}}(c) - i_d\right)^2\right). \tag{16}$$

The parameters α and β are positive scalar weighting factors. The states $v^f_{\text{appr}}(c)$ and $i^f_{\text{appr}}(c)$ are influenced by a vector c representing the commanded input current profile i_c of the catching solenoid. This is defined by $i_c = \Psi(\mathbf{h}, c)$, where Ψ is a B-spline curve interpolated by air gap $\mathbf{h}$ whose control points are in vector c of dimension n. The vector c is further constrained by c_{ub}, which interpolates the current profile produced under constant maximum input voltage, and c_{lb}, which interpolates the lowest current profile that still enables landing.

The EMV optimization problem then has no equality constraint and only two input inequality constraints in c_{lb} and c_{ub},

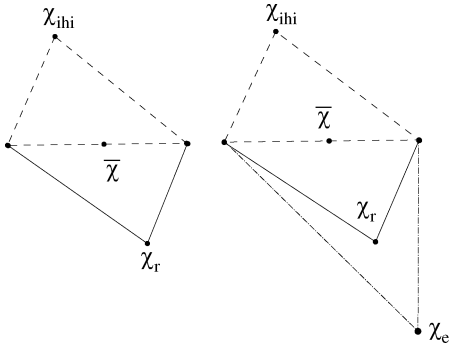

Fig. 4. Nelder Mead algorithm steps: (left) reflection and (right) expansion.

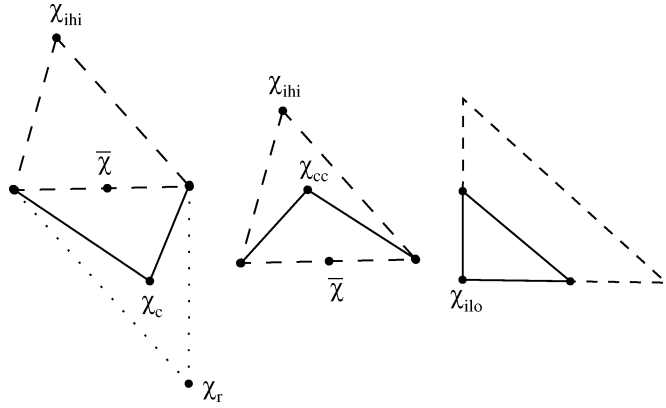

Fig. 5. Nelder Mead algorithm steps: (left) contraction outside, (middle) contraction inside, and (right) shrinkage.

which defines the highest and lowest current profiles that the search must stay within. The result is a nonlinear programming problem of the form

$$\begin{aligned} &\text{minimize} \quad F(c) \quad \text{w.r.t. to vector } c \\ &\text{subject to} \quad c_{lb}(j) \le c(j) \le c_{ub}(j) \quad \text{index } j = 1, \ldots, n \end{aligned}.$$

A. Nelder Mead Algorithm and Trial Point Determination

The Nelder Mead simplex method is a direct search nonlinear programming algorithm which does not need derivative information such as gradient or Hessian. While other derivative-free methods are available (e.g., pattern search, Rosenbrock's method, Powell's method, etc.), Nelder Mead is used because of its intuitiveness and computational efficiency [28]. For a detailed discussion on direct search methods, see [29].

Instead of taking the numerical gradient, the algorithm maintains a "non-degenerate simplex". The definition of a simplex is a set of $n+1$ points in n dimensions, i.e., if the input current profile is interpolated by n coefficients, then the simplex should have $n+1$ different current profiles. A simplex is non-degenerate if the vectors connecting any single vertex to the remaining vertices span the entire space. Non-degeneracy is important because Nelder Mead uses a linear combination of the connection vectors between vertices to search for lower-cost current profiles. During initialization, a simplex is created by perturbing every element of a vertex χ_1 by ϵ as

$$\begin{aligned} \chi_1 &= [\chi_{11} \quad \chi_{12} \quad \chi_{13} \quad \cdots \quad \chi_{1n}] \\ \chi_{j+1} &= [\chi_{11} \quad \cdots \quad \chi_{1j} + \epsilon \quad \cdots \quad \chi_{1n}] \end{aligned}$$

with $j = 1, \ldots, n$ for all $n+1$ vertices in the simplex.

How the Nelder Mead algorithm [30] searches for a local minimum using ordering and linear combination of the simplex vertices is illustrated in Figs. 4 and 5 for a simple 2-D system (three point simplex).

To find the next trial point, the simplex is reordered based on the result of functional evaluation $F(\chi)$. The "worst" vertex, χ_{ihi} is determined and is then moved toward the direction of the remaining vertices, represented by their average, $\overline{\chi}$ (see Fig. 4, left). If the function evaluation at the new point χ_r is lower, then the point is moved further in the same direction for potential reduction (see χ_e, Fig. 4, right). Otherwise, depending on the trial result, the next trial point can be moved back toward the "average" point (see χ_c, Fig. 5, left) or even past the "average" point toward the "worst" point (see χ_{cc}, Fig. 5, middle). When the "worst" vertex is replaced by a better vertex, the iteration ends. The goal is to eventually replace the "best" point, χ_{ilo}, in the simplex. If nothing better than the "worst" vertex can be found, the simplex itself can be shrunk toward its "best" vertex (see Fig. 5, right).

For the EMV system, $F(c)$ is determined via (16) using measurements of current and velocity at the end of approach control. Convergence occurs either when the cost function is reduced sufficiently or when the spacing within the simplex shrinks beyond a threshold. If the algorithm is stuck at a local minimum, the entire simplex can be reset through randomization. For real-time implementation in an interrupt routine, the algorithm is converted to a finite-state machine similar to [31].

B. Sine Coordinate Transformation and Computation

Sine coordinate transformation, [32], is implemented to ensure the solution from the Nelder Mead algorithm is realizable by the physical system. Suppose c is the optimization variable constrained by upper-bound c_{ub} and lower-bound c_{lb}.

Solving the optimization problem in c is equivalent to solving the unconstrained problem in z, which is related to c as

$$c = c_{lb} + (c_{ub} - c_{lb})\frac{(sin(z)+1)}{2}. \tag{17}$$

By inverting (17) and checking the necessary condition of arcsine, an expression for $z(i)$ can be found. Since the output from the sine function only varies between -1 and 1, modifying z will result in changing c within the maximum current profile c_{ub} and minimum current profile c_{lb}. This and the smoothness property of the B-spline mean that the resultant current profile would be realizable despite the ± 42 V input constraint.

To estimate the computational requirement from each method, the number of floating point operations (flops) are computed. Nelder Mead requires only 48 flops for each current profile while the nonlinear ILC (9) is around 750 flops. In Terminal ILC, (13) and (14) together require hundreds of flops.

C. Simulation Results

Simulation is used to determine the number of iterations required for v^f_{appr} and i^f_{appr} to converge when the Nelder Mead

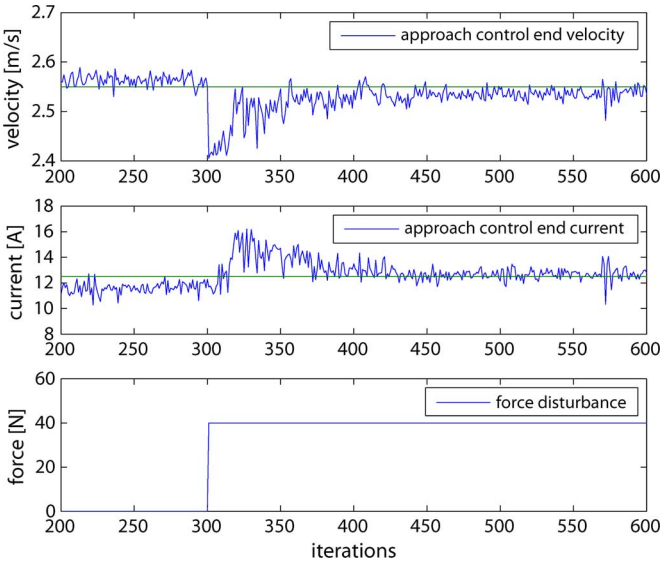

Fig. 6. Step disturbance simulation: (top) approach control end velocity, (middle) end current, and (bottom) disturbance force.

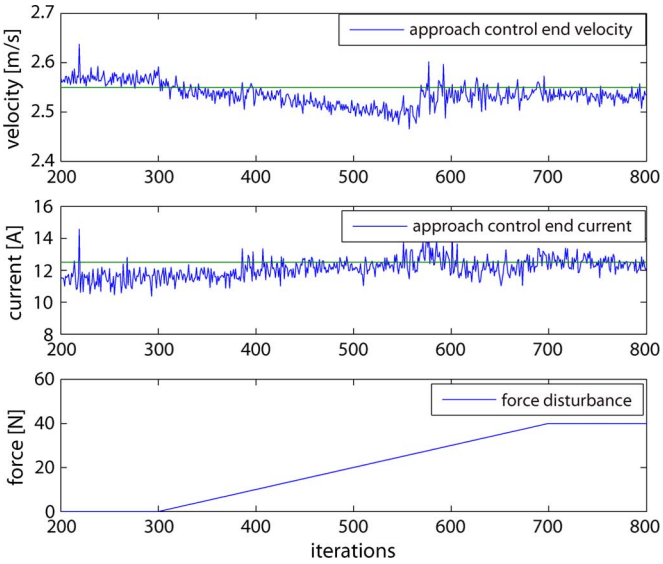

Fig. 7. Ramp disturbance simulation: (top) approach control end velocity, (middle) end current, and (bottom) disturbance force.

algorithm counters a step or ramp disturbance. The criteria for convergence is defined to be within $\pm 2\%$ of v_d and $\pm 5\%$ of i_d. In Fig. 6, a 40 N step increase of disturbance force occurs at step 300 and roughly 100 iterations are needed for both velocity and current to converge—a 40 N disturbance force corresponds to approximately a 15% engine load change on the exhaust valve. The response to a ramp disturbance of 40 N force over 400 valve cycles is shown in Fig. 7. Despite the fact that simplex vertices become obsolete quickly under a ramp disturbance, the deviation from velocity setpoint is still within 0.1 m/s.

V. Experimental Setup

The experimental setup is shown in Fig. 8. On the right is the solenoid valve attached to a workbench and connected to a

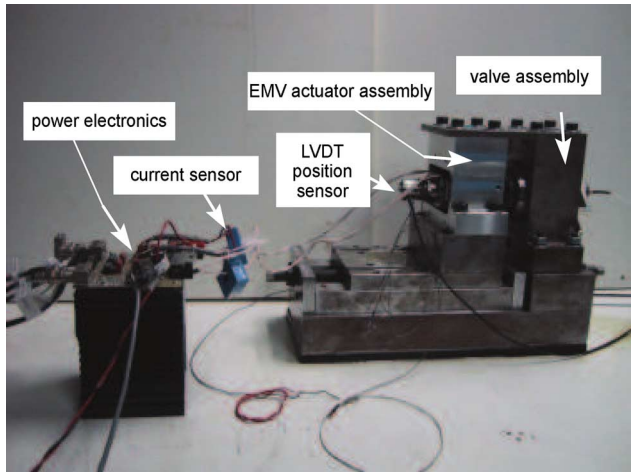

Fig. 8. Electromechanical valve actuator test-bench setup with power electronics and sensors.

linear variable differential transformer (LVDT) position sensor. On the left is the H-bridge power electronic that provides three output modes (± 42, 0 V) for pulse width modulation output by switching two insulated gate bi polar transistors. Integrated in the power electronics are two Hall effect current sensors (LA55-P from LEM S.A.). Not shown, are the ± 15 V power supply for the current sensors and the Sorenson power supply (DCS60-18E) powering the H-bridge. The control software is implemented in C on dSPACE DS1103 hardware at 50 kHz. Data monitoring and acquisition are performed on a PC host through dSPACE ControlDesk software.

VI. Experimental Results

Only experimental results with the Nelder Mead approach controller are presented in this section.

A. Unknown Disturbance Regulation

Even under laboratory condition, the open-loop terminal approach velocity v^f_{appr} changes over time due to unknown varying disturbances. The Nelder Mead controller performance over 4000 continuous cycles results in an average velocity of $v_d = 2.6$ m/s and variance of $\sigma_{NM} = 2 \cdot 10^{-5}$ m^2/s^2, which is a reduction by a factor of 3.45 compared to the result without controller adaptation ($\sigma_{OL} = 6.9 \cdot 10^{-5}$m^2/s^2), as seen in the histogram comparison in Fig. 9.

B. Cold Start

When the EMV actuator is first activated, the increase in temperature (due to coil ohmic losses) affects the mechanical damping and the electromagnet. The requirement on the approach controller is that it should regulate the speed of armature to the desired point as quickly as possible during a cold start and then adapt the control to maintain the set point as the system warms up. Fig. 10 shows that the Nelder Mead controller regulates the velocity to near the 2.6 m/s setpoint in 150 iterations while the open-loop controller takes 700 iterations to reach 2.6 m/s velocity.

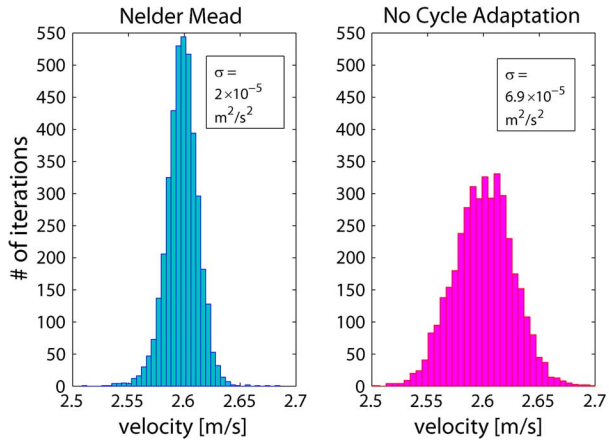

Fig. 9. Histogram of approach control end velocity after 4000 iterations with variances (σ) listed: (left) with and (right) without Nelder Mead adaptation.

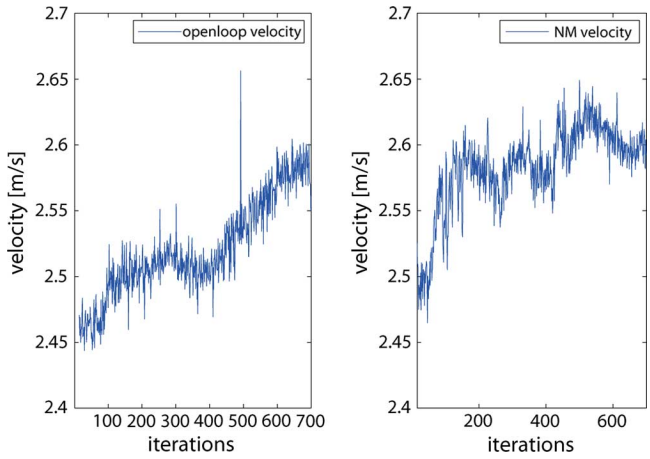

Fig. 10. Cold start performance with and without Nelder Mead cycle adaptation: regulating velocity at the end of approach control.

C. Regulate Against Force Change

Since the disturbance in Section IV-A is unknown, it is impossible to quantify how well the algorithm rejects disturbances. To simulate a known disturbance force, the release solenoid is used to hold back the armature as if cylinder pressure is present—the cylinder pressure acts on the valve area to produce a force on the EMV.

1) Simulation of In-Cylinder Pressure: Back pressure at different loads on an engine has been measured experimentally. Since the force on the valve is area times the back pressure, setting the current of the release magnet to achieve the same force profile mimics the real back pressure. The current profile required to generate the magnetic force was determined by finite element simulation work reported in [22] and [33], and the maximum force simulated is kept less than 77 N (corresponding to 1.5 bars pressure acting on the valve) to keep the required current in the release magnet within a safe level. Since most of the gas exchange and pressure equalization occur during the initial part of the motion in a real engine, the force imposed on the valve by cylinder pressure can be effectively simulated using

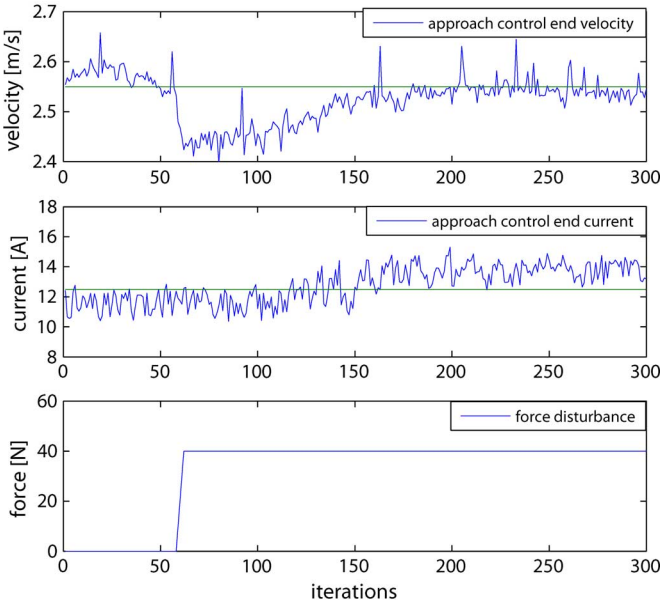

Fig. 11. Step disturbance experiment: (top) approach control end velocity, (middle) end current, and (bottom) force.

the release coil for this engine despite the limited force at larger air gaps.

2) Step Force Change: Fig. 11 shows that approximately 120 cycles are needed to regulate v^f_{appr} back to within $\pm 2\%$ of the desired velocity, v_d, for a force increase of 40 N (representing roughly 15% of a full load step for the exhaust valve). The cycle by cycle system responses to the disturbance in Fig. 11 compare quite well to the simulation of the same case shown in Fig. 6. The simulation and experimental results for a step disturbance of -40 N also have a convergence time of approximately 100 to 150 iterations as shown in [27].

3) Ramp Disturbance: During a ramp disturbance, the controller can be misled by obsolete vertices that carry lower cost values, and results in producing a series of inferior trial points. Since the disturbance is much slower than the valve travel time, the rate of ramp disturbance is slow, limiting the effect of obsolete vertices. Fig. 12 shows that the increasing force ramp of 30 N over 300 valve cycles, does not affect the terminal conditions due to the controller regulation. The experimental results in Fig. 12 again match well with the simulation results in Fig. 7. For the negative ramp case, the controller also handles a rate of up to 10 N per 100 valve cycles both in simulations and in experiments—see [27].

D. Input Coefficient Evolution and Cost Function

The top graph of Fig. 13 shows the evolution of the current input versus air gap. The dotted lines are transient profiles during the search process. The middle and bottom plots confirm that the controller regulates the end conditions to the desired set-point during these iterations. In Fig. 13, the Nelder Mead controller raises the current profile to counter a step increase of

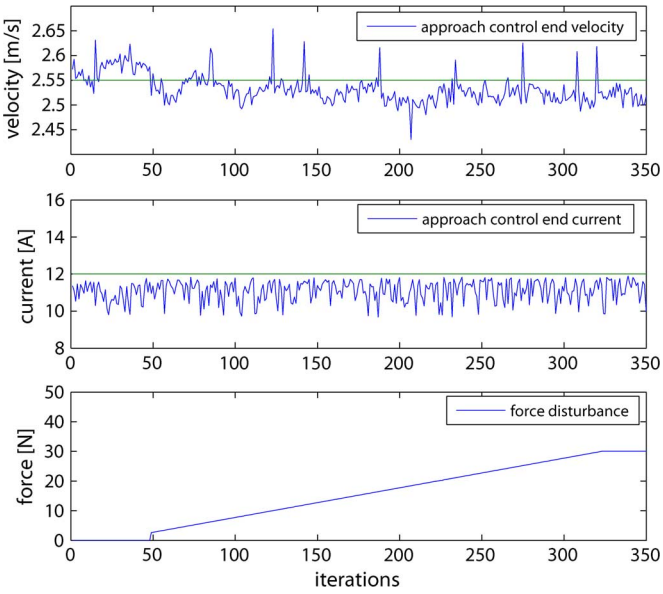

Fig. 12. Ramp disturbance experiment: (top) approach control end velocity, (middle) end current, and (bottom) force.

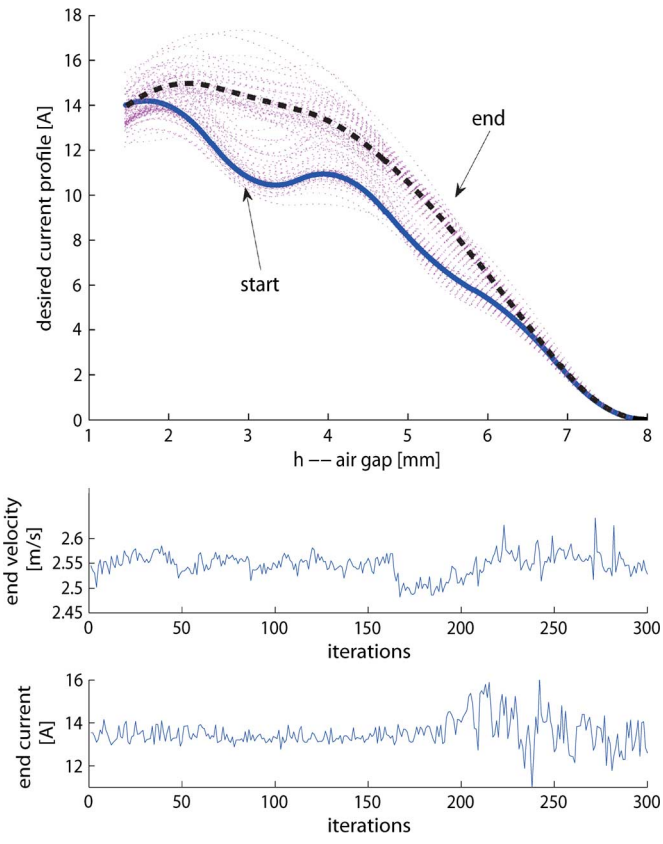

Fig. 13. Nelder mead controller regulating against a 20 N step disturbance force at iteration 160: (top) evolution of command current profile; (middle and bottom) approach control end velocity and current with respect to iterations.

20 N force disturbance at iteration 160, and maintains the velocity/current end state.

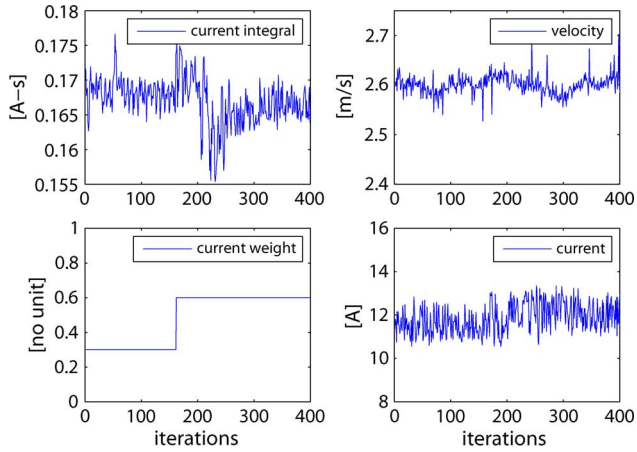

Fig. 14. Cost function experiment with current integral weight changes: (top left) current integral, (bottom left) current weighting in cost function, (top right) approach control end velocity, (bottom right) end current.

Modifying the cost function by adding the current integral, representing electric energy, the Nelder Mead controller can be directed to reduce energy consumption

$$F(c) = \left(\alpha \left(v^f_{\text{appr}} - v_d\right)^2 + \beta \left(i^f_{\text{appr}} - i_d\right)^2\right) + \gamma \int_0^{t_{\text{end}}} i(t)dt.$$

Fig. 14 shows that by increasing the current weight γ in the cost function $F(c)$, the current integral can be reduced without introducing errors to the v^f_{appr} and i^f_{appr}. Using the modified cost function, the current integral per valve event is slightly reduced from 0.169 to 0.166 As.

VII. Conclusion

To reduce the seating impact of an electromagnetic valve actuator (EMV), approach control is investigated. The common goal of the approach controllers is to ensure that the subsequent landing trajectory has the desired initial conditions. This improves the valve-seating performance, as measured by the impact velocity, since the landing control is sensitive to initial conditions. Two iterative learning controllers are considered but they do not perform well because their structures do not handle saturation despite the nonlinear convergence proof and feedback linearization. However, both simulation and experiment results indicate that after 100 to 150 valve cycles, the Nelder Mead controller rejects the effect of step disturbance force of 40 N (equivalent to ∼15% of a full load step on the exhaust valve). A ramp disturbance force of 10 N per 100 valve cycles is also rejected. In addition, the electric energy consumption can be reduced if a current integral term is added to the cost function. The Nelder Mead controller produces satisfactory results in terms of optimization capability, robustness against disturbances, and computational efficiency for the EMV approach control.

VIII. Future Work

The Nelder Mead approach controller presented here should be combined with a feedback landing controller (e.g., [8] or

[19]) to solve the overall valve-seating problem. To handle fast in-cylinder pressure changes, an approach to combine the Nelder Mead controller and a disturbance estimator based feedforward controller such as [13] could be investigated.

REFERENCES

[1] H. Hong, G. Parvate-Patil, and B. Gordon, "Review and analysis of variable valve timing strategies—Eight ways to approach," *Proc. Inst. Mech. Eng. D, J. Automob. Eng. (U.K.)*, pp. 1179–1200, 2004.

[2] M. Pischinger, W. Salber, F. van der Staay, H. Baumgarten, and H. Kemper, "Benefits of the electromechanical valve train in vehicle operation," SAE, Warrendale, PA, Paper No. 2000-01-1223, 2000.

[3] M. Schechter and M. Levin, "Camless engine," SAE, Warrendale, PA, Paper No. 1996-05-81, 1996.

[4] Z. Sun and D. Cleary, "Dynamics and control of an electro-hydraulic fully flexible valve actuation system," in *Proc. Amer. Control Conf.*, 2003, pp. 3119–3124.

[5] J. Zhao and R. Seethaler, "A fully flexible valve actuation system for internal combustion engines," *IEEE/ASME Trans. Mechatronics*, vol. 16, no. 2, pp. 361–370, Apr. 2011.

[6] C. Weddle and D. Leo, "Embedded actuation system for camless engines," in *Proc. Int. Conf. Adaptive Structure Tech.*, 1998, pp. 294–303.

[7] J. Ma, G. Zhu, H. Schock, and J. Winkelman, "Adaptive control of a pneumatic valve actuator for an internal combustion engine," in *Proc. Amer. Control Conf.*, 2007, pp. 3678–3685.

[8] S. K. Chung, C. R. Koch, and A. F. Lynch, "Flatness-based feedback control of an automotive solenoid valve control," *IEEE Trans. Control Syst. Technol.*, vol. 2, pp. 394–401, Mar. 2007.

[9] Y. Wang, T. Megil, M. Haghgooie, K. Peterson, and A. Stefanopoulou, "Modeling and control of electromechanical valve actuator," SAE, Warrendale, PA, Paper No. 2002-01-1106, 2002.

[10] S. K. Chung, "Flatness-based end-control of a gas exchange solenoid actuator for IC engines," M.S. thesis, Univ. Alberta, Dept. Mech. Eng., , Edmonton, AB, Canada, 2005.

[11] K. Peterson and A. Stefanopoulou, "Extremum seeking control for soft landing of an electromechanical valve actuator," *Automatica*, vol. 40, no. 6, pp. 1063–1069, 2004.

[12] J. Savage and J. Matterazzo, "Application of design of experiments to determine the leading contributors to engine valvetrain noise," SAE, Warrendale, PA, Paper No. 1993-08-84, 1993.

[13] R. R. Chladny and C. R. Koch, "Flatness-based tracking of an electromechanical VVT actuator with disturbance observer feed-forward compensation," *IEEE Trans. Control Syst. Technol.*, vol. 16, no. 4, pp. 652–663, Jul. 2008.

[14] S. Butzmann, J. Melbert, and A. Koch, "Sensorless control of electromagnetic actuators for variable valve train," SAE, Warrendale, PA, Paper No. 2000-01-1225, 2000.

[15] C. Tai and T. Tsao, "Control of an elctromechanical actuator for camless engines," in *Proc. Amer. Control Conf.*, 2003, pp. 3113–3118.

[16] C. Gunselmann and J. Melbert, "Improved robustness and energy consumption for sensorless electromagnetic valve train," SAE, Warrendale, PA, Paper No. 2003-01-0030, 2003.

[17] M. Montanari, , F. Ronchi, C. Rossi, and A. Tonielli, "Control of a camless engine electromechanical actuator: Position reconstruction and dynamic performance analysis," *IEEE Trans. Ind. Electron.*, vol. 15, no. 2, pp. 299–311, Apr. 2004.

[18] I. Haskara, V. Kokotovic, and L. Mianzo, "Control of an elctro-mechanical valve actuator for a camless engine," *Int. J. Robust Nonlinear Control*, vol. 14, pp. 561–579, 2004.

[19] P. Eyabi and G. Washington, "Modeling and sensorless control of an electromagnetic valve actuator," *IEEE J. Mechatron.*, vol. 16, pp. 159–175, 2006.

[20] W. Hoffmann, K. Peterson, and A. G. Stefanopoulou, "Iterative learning control for soft landing of electromechanical valve actuator in camless engines," *IEEE Trans. Control Syst. Technol.*, vol. 11, no. 2, pp. 174–184, Mar. 2003.

[21] K. S. Peterson, "Control methodologies for fast and low impact electromagnetic actuators for engine valves," Ph.D. dissertation, Dept. Mech. Eng., Univ. Michigan, Ann Arbor, 2005.

[22] R. R. Chladny, C. R. Koch, and A. F. Lynch, "Modeling automotive gas-exchange solenoid valve actuator," *IEEE Trans. Magn.*, vol. 41, no. 3, pp. 1155–1162, Mar. 2005.

[23] M. Sun, D. Wang, and Y. Wang, "Sampled-data iterative learning control with well-defined relative degree," *Int. J. Robust Nonlinear Control (U.K.)*, vol. 14, no. 8, pp. 719–739, May 2004.

[24] J.-X. Xu, Y. Chen, T. H. Lee, and S. Yamamoto, "Terminal iterative learning control with an application to RTPCVD thickness control," *Automatica*, vol. 35, no. 9, pp. 1535–1542, 1999.

[25] G. Oriolo, S. Panzieri, and G. Ulivi, "Learning optimal trajectories for nonholonomic systems," *Int. J. Control*, vol. 73, no. 10, pp. 980–991, Jul. 2000.

[26] R. Corless, G. H. Gonnet, D. E. G. Hare, D. J. Jeffrey, and D. E. Knuth, "On the Lambert W function," *Adv. Comput. Maths*, vol. 5, pp. 329–359, 1996.

[27] J. Tsai, "Approach control of a gas exchange solenoid actuator for IC engines," M.S. thesis, Sch. Eng. Sci., Simon Fraser Univ., Burnaby, BC, Canada, 2007.

[28] J. Lagarias, J. A. Reeds, M. H. Wright, and P. E. Wright, "Convergence properties of the Nelder-Mead simplex method in low dimensions," *SIAM J. Optimization*, vol. 9, no. 1, pp. 112–147, 1998.

[29] R. Lewis, V. Torczon, and M. Trosset, "Direct search methods: Then and now," *J. Comput. Appl. Math.*, vol. 124, no. 1–2, pp. 191–207, 2000.

[30] E. Polak, *Computational Methods in Optimization: A Unified Approach*. New York: Academic Press, 1971.

[31] F. Sigworth, "State-machine simplex minimizer," 2003. [Online]. Available: http://www.mathworks.com/matlabcentral/fileexchange

[32] J. D'Errico, "Understanding fminsearchbnd," 2005. [Online]. Available: http://www.mathworks.com/matlabcentral/fileexchange

[33] R. Chladny, "Modeling and simulation of automotive gas exchange valve," M.S. thesis, Dept. Mech. Eng., Univ. Alberta, Edmonton, AB, Canada, 2003.